Ternary Thiol−Ene/Acrylate Photopolymers: Effect of Acrylate Structure on Mechanical Properties

Askim F. Senyurt,[†] Huanyu Wei,[†] Charles E. Hoyle,*[,†] Scott G. Piland,[‡] and Trenton E. Gould[‡]

School of Polymers and High Performance Materials and School of Human Performance and Recreation, University of Southern Mississippi, 118 College Drive, 10076 Hattiesburg, Mississippi 39406

Received November 2, 2006; Revised Manuscript Received March 14, 2007

ABSTRACT: Model ternary thiol−ene/acrylate photopolymerization involving acrylate homopolymerization and copolymerization of thiol−ene and thiol−acrylate monomers were monitored by real-time FTIR. In all ternary mixtures, including those prepared with different acrylate concentrations, acrylate conversion was 100%. However, thiol−ene conversions were found to be controlled by their initial concentrations. The influence of acrylate monomer chemical structure on the thermophysical properties of ternary thiol−ene/acrylate systems was studied with DMA, DSC, and the absorbance of a nondestructive impact energy. The addition of acrylate to the thiol−ene system increased the rubbery modulus while the tan δ_{max} shifted to higher temperatures. Densely cross-linked, heterogeneous matrix formation was observed with the broadening of tan δ peaks at high acrylate concentrations. The high impact absorption of these ternary thermoset photopolymers was correlated with the dynamic mechanical damping ability of the networks. Acrylates with higher functionality and low molecular weight per double bond are more effective at increasing the glass transition temperature of the thiol−ene polymer network. Fracture behavior of ternary thiol−ene/acrylate networks under impact shows a dependence on the chemical structure of the acrylate, component concentrations, and low-temperature relaxation processes. The ternary matrix formed with a bisphenol A based difunctional acrylate monomer exhibited improved impact energy absorption at room temperature. Finally, tensile properties of polymer networks formed with thiol−ene/acrylate and thiol−acrylate mixtures are given for comparison purposes.

Introduction

Photopolymerization continues to advance due to the use of solvent-free formulations, rapid cure rates, and low-energy consumption. Acrylates are the most commonly used photocurable materials. Photopolymerization of multifunctional acrylates forms thermoset materials, finding application areas ranging from protective films on floors and wood to coatings on compact discs, and optical fibers.[1] Radicals produced by exposure to light initiate the chain growth addition reaction of acrylic monomers. In chain growth polymerization of multifunctional acrylates, heterogeneous high-density regions are formed at low double bond conversion,[2−6] ultimately resulting in heterogeneous networks upon macrogelation at higher conversions. Acrylate polymerization is also inhibited by oxygen.[1−6]

Thiol−ene systems are an alternative class of monomers that form structurally homogeneous networks via a step-growth free-radical process[7−20] that leads to high monomer conversions, low shrinkage,[8−10] homogeneity in mechanical properties,[8−15] photoinitiator-free formulations,[9−11,17−19] and very little oxygen inhibition.[8−11,20] For enes that do not homopolymerize, thiol−ene reactions proceed via the propagation reaction of a thiyl radical with a terminal ene monomer to form a carbon-centered radical. This radical, in the absence of a propagation reaction with another ene monomer, chain transfers to a thiol monomer by a hydrogen abstraction process. The rate-determining step is dependent upon the type of ene monomer used in the reaction. There have been several reports[7−11,18,21−26] that deal with the kinetics of these two-step reaction mechanisms related to the overall reaction order, calculation of kinetic constants, and the dependence of polymerization rate on monomer concentration and chemical structure. There are only a few papers[9−11,14,29] that examine the thermal and mechanical properties of the cross-linked networks formed from the polymerization of thiol−ene systems.

In order to modify the basic structure inherent to acrylate networks, multifunctional thiols have been added to acrylate monomers.[8,11,27−29] When a multifunctional thiol is added to a multifunctional acrylate monomer, a competition exists between the step-growth thiol−acrylate copolymerization process and the chain-growth acrylate homopolymerization. Homopolymerization of acrylate groups combined with thiol−acrylate reactions results in a more homogeneous, mechanically uniform cross-linked network with a narrow glass transition region and a lower glass transition temperature.[11] Other advantages of the thiol addition to acrylates include decreased shrinkage and reduced oxygen inhibition.[8,11,27−29] The concentration of added thiol, the conversion of thiol and acrylate monomers, and the type of propagation mechanism control the structure and properties of the final cross-linked matrix.[8,11,27−29]

Recently, Cramer et al.[25] published a paper dealing with the kinetic modeling of ternary thiol−ene systems: thiol−ene−ene and thiol−ene/acrylate. They characterized the polymerization of two sets of thiol−ene−ene systems in which the ene monomers do not homopolymerize: a tetrafunctional thiol copolymerization with a divinyl ether and a multinorbornene and a tetrafunctional thiol copolymerization with a diallyl ether and a multinorbornene. It was shown that the ene monomers did not cross-polymerize during the reaction and that thiol was

* To whom correspondence should be addressed: e-mail charles.hoyle@usm.edu; Ph 601-266 4873; Fax 601-266 5504.
[†] School of Polymers and High Performance Materials.
[‡] School of Human Performance and Recreation.

10.1021/ma062534b CCC: $37.00
Published on Web 06/19/2007

Chart 1. Chemical Structures of Thiol−Ene Monomers: (a) APE and (b) TriThiol

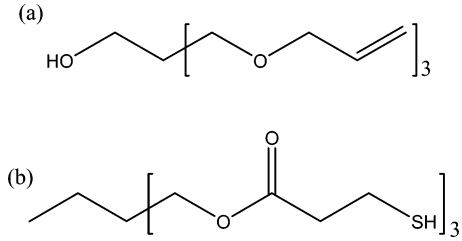

consumed by addition to the ene monomers dictated by the propagation kinetic parameter of each reaction. On the other hand, in the thiol−vinyl ether/acrylate polymerization, the thiol is twice as likely to react with the vinyl ether as the acrylate, and the presence of the thiol eliminates the acrylate/vinyl ether cross-propagation reaction.

Herein, we report a detailed investigation of ternary thiol−ene/acrylate systems that considers both functional group conversions and the final material physical and mechanical properties. A model kinetic real-time FTIR study was first conducted with a representative trifunctional thiol, triallyl ether, and triacrylate. An extensive analysis of thermal and mechanical properties, i.e., mechanical relaxation spectra (tan δ) and nondestructive impact energy absorption, was carried out on this ternary system as a function of triacrylate concentration. Next, the chemical structure of the acrylate was varied systematically to study the effect on network formation and final polymer properties. More specifically, these materials were examined for their nondestructive energy-absorbing properties at room temperature. Networks with high-energy absorption under action of a nondestructive impact force have potential importance in a variety of athletic and other personnel protection applications where impact energies less than required to produce material failure are routinely encountered. The result of this study is the establishment of a relationship between the chemical structure of the monomers and the mechanical properties of the final cross-linked networks. This paper is a detailed extension of a brief communication on the mechanical and physical properties of a ternary thiol−ene/acrylate system.[30]

Experimental Section

Materials. Trimethylolpropane tris(3-mercaptopropionate) (TriThiol) and allyl pentaerythritol (APE) were donated by Bruno Bock ThioChemical-S and Perstorp Specialty Chemicals, respectively. Acrylates used in this study, propoxylated glycerol triacrylate (Acr1), trimethylolpropane triacrylate (Acr2), pentaerythritol tetraacrylate (Acr3), dipentaerythritol pentaacrylate (Acr4), ethoxylated trimethylolpropane triacrylate (Acr5), ethoxylated pentaerythritol tetraacrylate (Acr6), and ethoxylated bisphenol A diacrylate (Acr7), were obtained from Cytec Surface Specialties and Sartomer Company. 2,2-Dimethoxy-2-phenylacetophenone (DMPA) was obtained from Ciba Specialty Chemicals. All chemicals (Chart 1 and Chart 2) were used as received without further purification.

Sample Preparation for Testing. Thiol−ene mixtures were prepared by blending TriThiol with APE based on equal molar functional groups. Acrylates were then added to the thiol−ene mixture in different mole percentages. A photoinitiator (DMPA) concentration of 0.02 wt % of the total thiol−ene/acrylate monomers mixture was added to ensure adequate through curing. DMPA was first dissolved in the TriThiol before mixing with the ene monomer. Subsequently, the acrylate was added.

Thick 4 mm plates (impact and thermal testing) and 1 mm thick plates (tensile testing) were irradiated with the output of a 305 nm low-pressure mercury lamp (light intensity ~0.1 mW/cm^2) in air followed by exposure to a Fusion light source (see below for description). UV light intensity of the low-pressure lamp at the

Chart 2. Chemical Structures of Acrylates: (I) Propoxylated Glycerol Triacrylate (Acr1), (II) Trimethylolpropane Triacrylate (Acr2), (III) Pentaerythritol Tetraacrylate (Acr3), (IV) Dipentaerythritol Pentaacrylate (Acr4), (V) Ethoxylated Trimethylolpropane Triacrylate (Acr5), (VI) Ethoxylated Pentaerythritol Tetraacrylate (Acr6), and (VII) Ethoxylated Bisphenol A Diacrylate (Acr7)

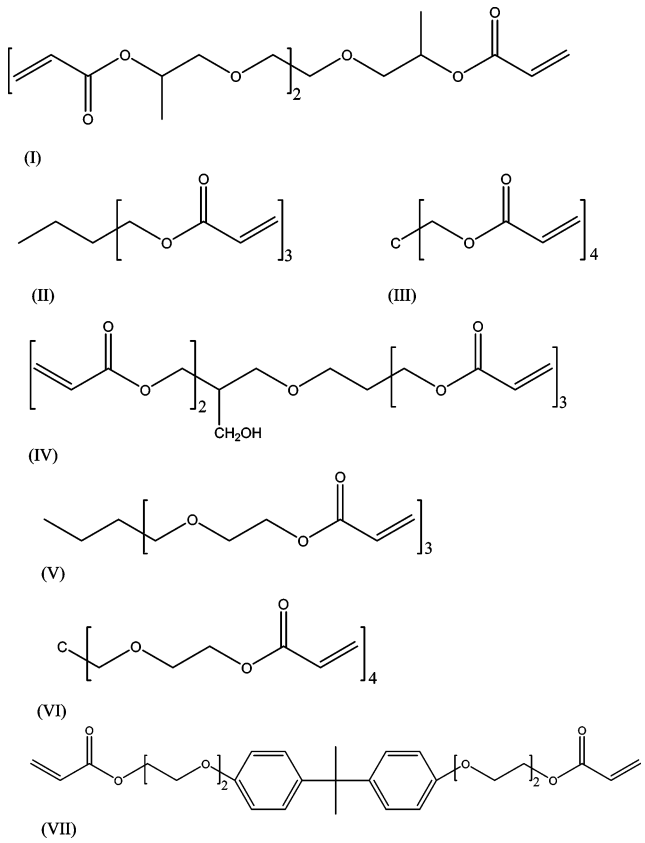

samples was measured by a calibrated radiometer (International Light IL-1400). Samples were thus first cured (initially intermittently to reduce heat build up on sample) for a total of 30 min to ensure high conversion of functional groups before passing under the Fusion lamp source (UV Fusion line EPIQ 6000 with D bulb and intensity of 3.146 W/cm^2 at a line speed of 3 m/min; 10 passes: 5 front side and 5 back side). As an indication of the functional group conversion uniformity (front to back) of the various types of 4 mm plates cured by this methodology, the allyl ether and acrylate double bond conversions at the front (1 mm section), middle (1 mm section), and back (1 mm section) of the cured plates were determined to be 100% for the TriThiol-APE 4 mm sample by monitoring the intensity of the allyl ether ene and acrylate bonds at 6120 and 6160 cm^{-1}, respectively, with an internal standard at 5790 cm^{-1}. The 4 mm 25% TriThiol−25% APE/50% Acr1 sample acrylate conversion was 100% conversion at the top, center, and back of the plate while the allyl ether ene conversions were 74%, 73%, and 74%, respectively.

Kinetic analyses were conducted with real-time FTIR (RTIR) to obtain conversions of all components in the thiol−ene/acrylate mixtures. The conversion as a function of irradiation time was recorded on a modified Bruker 88 spectrometer with a 200 W high-pressure mercury−xenon lamp source. The infrared absorption spectra were obtained under continuous UV irradiation at a scanning rate of 4 scans/s. In the RTIR measurements, polymerization was initiated with a light intensity of 1.87 mW/cm^2. The thiol group conversion was monitored by measuring the area under the peak of the 2570 cm^{-1} band, while the peaks at 812 and 3064 cm^{-1} were used to measure the acrylate and allyl ether double bond conversions, respectively. Acrylate has a distinctive infrared absorbance at 812 cm^{-1}, while the allyl ether infrared absorbance at 3064 cm^{-1} overlaps with an acrylate band. Since the absorbance

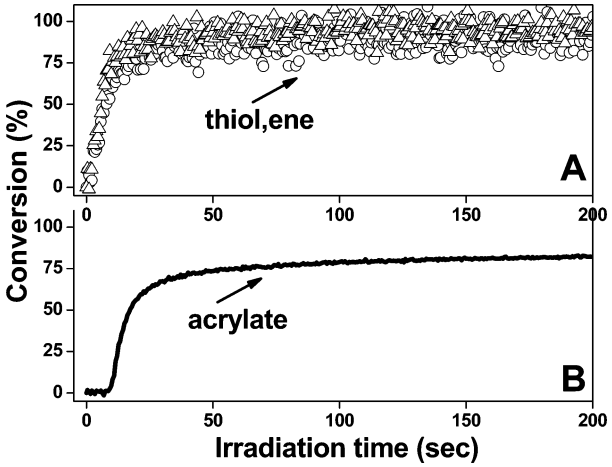

Figure 1. RTIR conversions for (A) 1:1 molar mixtures of TriThiol (○) and APE (Δ) and (B) Acr1 in air with 1.0 wt % DMPA (light intensity 1.87 mW/cm^2 at 365 nm; high-pressure mercury−xenon lamp source).

ratio of the 812 and 3064 cm^{-1} is a constant value, the contribution of acrylate at 3064 cm^{-1} can be calculated from the absorbance at 812 cm^{-1} and the allyl ether conversion can be obtained by subtracting the contribution of acrylate at 3064 cm^{-1}.

Thermal and Mechanical Testing. Thermal transitions of the polymerized thick plates were recorded using a TA Q800 dynamic mechanical analysis (DMA) by heating the samples from −120 to 120 °C at a rate of 2 °C/min and at a frequency of 1 Hz in air. DMA was conducted using the cantilever bending mode with specimen dimensions set at 35 mm × 12 mm × 4 mm (L × W × H). A differential scanning calorimetry (DSC, TA Q1000) was used to monitor thermal transitions by heating/cooling 5−10 mg samples at a rate of 10 °C/min under a nitrogen flow. The glass transition temperature is obtained from the second run of a heating cycle.

The energy absorbed upon impact was estimated to a first approximation[31] using a modified Tinius Olsen instrument, with the impact energy set at 1.13 J. The typical sample dimensions were 80 mm × 20 mm × 8 mm (L × W × H); two photocured 4 mm plates pressed together back to back to eliminate any contribution from the steel plate. The striking edge of the pendulum, which complied with ASTM 12.3, was made of hardened steel, tapered to have an incline angle of 45° and rounded at the edge to a radius of 3.17 mm. An infrared thermometer (Fisher Scientific) was used to measure the temperature of the samples before each impact absorption measurement.

Tensile property measurements were obtained with a mechanical testing machine (MTS-Alliance RT/10). Tensile properties were determined according to ASTM D882, using a 100 N load cell and a specimen gauge length of 50 mm at a crosshead speed of 25 mm/min. A width−thickness sample ratio of 8 was used for the tensile testing.

Results and Discussion

Herein, the polymerization kinetics and physical and mechanical properties of several thiol−ene/acrylate systems are described in detail. All components are given in Charts 1 and 2. The goal is to provide a comprehensive rationale for structure−property relationships between the molecular components and the nature of the matrices generated as well as nondestructive impact energy absorbance and fracture formation of the photopolymerized networks.

Kinetics of TriThiol−APE/Acr1. Kinetic analyses were first conducted on Acr1 and a base binary system comprised of a 1:1 molar functional group mixture of TriThiol−APE with real-time FTIR (RTIR) in order to determine the effect of acrylate concentration on the thiol−ene/acrylate polymerization. Conversion vs time plots of TriThiol-APE and pure Acr1 (Figure 1, A and B, respectively) reveals that the acrylate monomer conversion is slower than thiol−ene conversion and reaches 80%, with an induction period due to oxygen inhibition. The thiol−ene conversions for the TriThiol−APE mixture are identical, reaching about 95% with no induction time. Obviously, TriThiol−APE copolymerizes in a 1:1 thiol:ene stoichiometric ratio. Upon the addition of Acr1, which can readily homopolymerize, to a TriThiol−APE mixture, the chain-growth homopolymerization of acrylate occurs along with the thiol−ene step-growth copolymerizations of thiol with both allyl ether and acrylate groups. In all the ternary mixtures prepared with

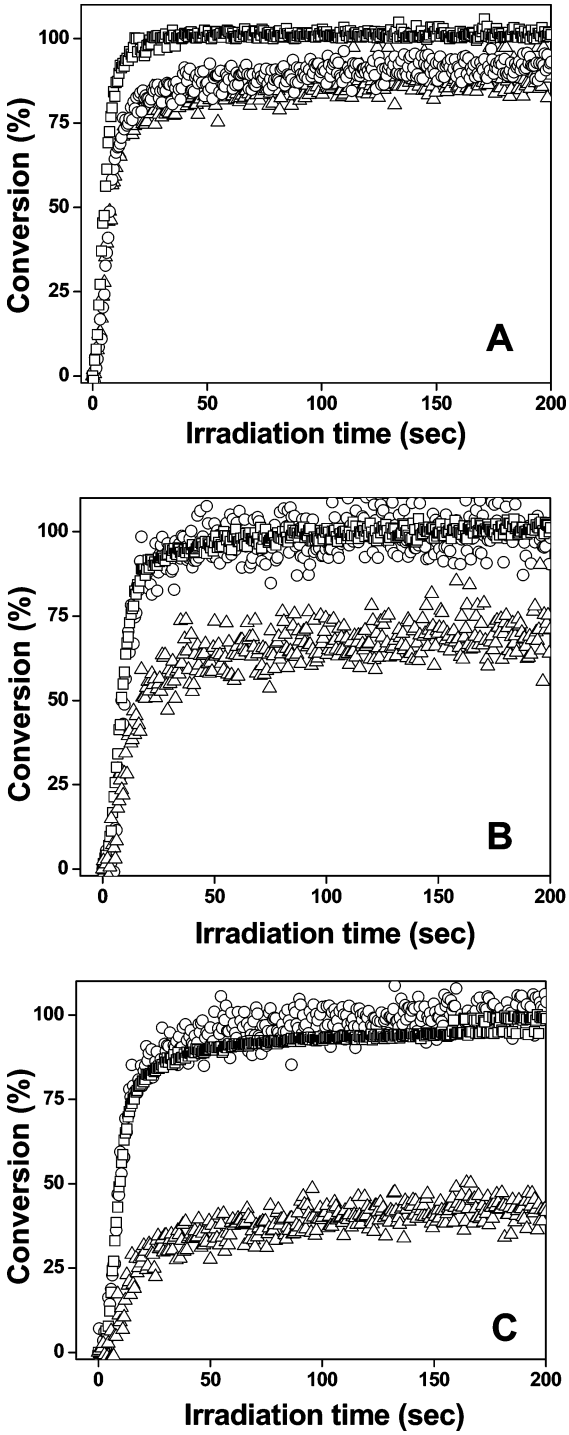

Figure 2. RTIR conversions of (A) 40% TriThiol−40% APE/20% Acr1, (B) 25% TriThiol−25% APE/50% Acr1, and (C) 15% TriThiol−15% APE/70% Acr1 (TriThiol (○), APE (Δ), and Acr1 (□)) in air with 1.0 wt % DMPA (light intensity 1.87 mW/cm^2 at 365 nm; high-pressure mercury−xenon lamp source).

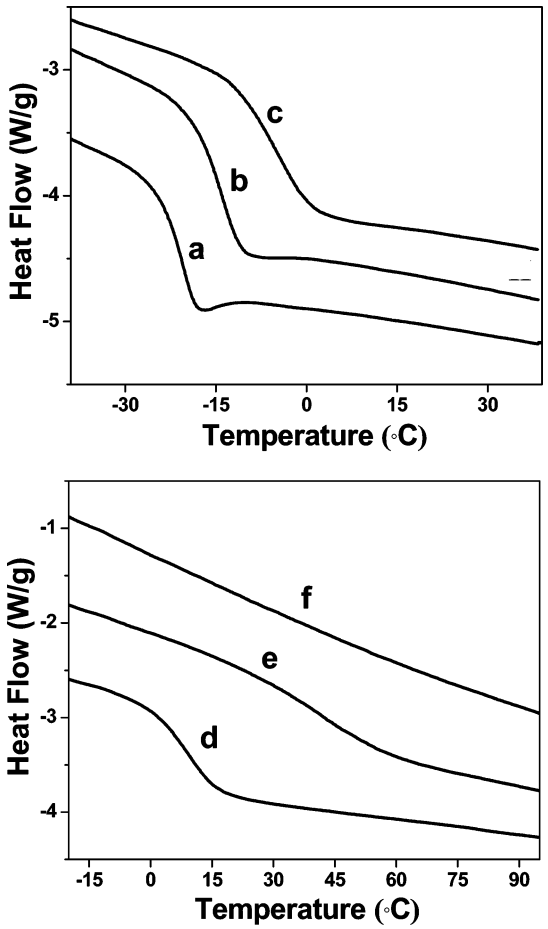

Figure 3. Thermal transitions of TriThiol−APE/Acr1 ternary films cured (see Experimental) in air: (a) TriThiol−APE, (b) 40% TriThiol−40% APE/20% Acr1, (c) 30% TriThiol−30% APE/40% Acr1 (III), (d) 25% TriThiol−25% APE/50% Acr1 (IV), (e) 10% TriThiol−10% APE/80% Acr1, and (f) Acr1 obtained with DSC, scanning rate of 10 °C/min.

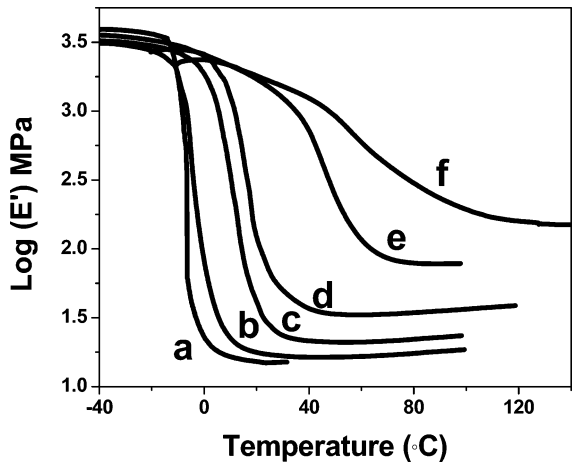

Figure 4. Storage moduli of TriThiol−APE/Acr1 ternary samples cured (see Experimental) in air: (a) TriThiol−APE, (b) 40% TriThiol−40% APE/20% Acr1, (c) 30% TriThiol−30% APE/40% Acr1, (d) 25% TriThiol−25% APE/50% Acr1, (e) 10% TriThiol−10% APE/80% Acr1, and (f) Acr1, obtained with DMA, at a scan rate 2 °C/min.

different Acr1 concentrations, acrylate conversion was 100% due to a combination of the homopolymerization of acrylate groups and their copolymerization with the thiol groups of TriThiol. However, thiol and allyl ether ene conversions are dependent on their initial concentrations, as shown in Figure 2. In the case of the 40% TriThiol−40% APE/20% Acr1 sample

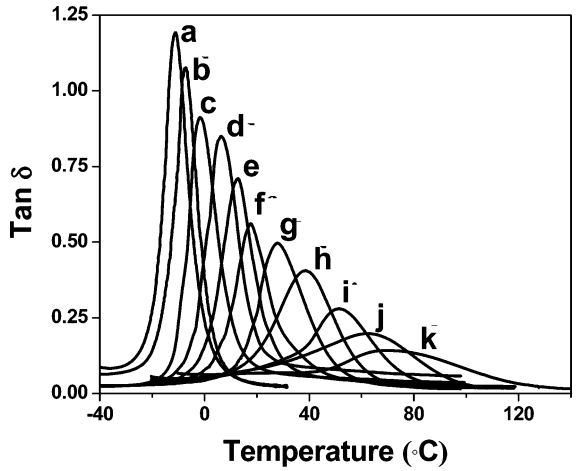

Figure 5. Tan δ plots of TriThiol−APE/Acr1 ternary samples cured (see Experimental) in air: (a) TriThiol−APE, (b) 10% Acr1, (c) 20% Acr1, (d) 30% Acr1, (e) 40% Acr1, (f) 50% Acr1, (g) 60% Acr1, (h) 70% Acr1, (i) 80% Acr1, (j) 90% Acr1, and (k) Acr1, obtained with DMA, at a scan rate 2 °C/min.

(Figure 2A), thiol and allyl ether reached 90% conversions. For the sample containing 25% TriThiol−25% APE/50% Acr1 (Figure 2B), acrylate and thiol groups were completely consumed during the polymerization, while allyl ether conversion reached 75%. On the other hand, in the mixtures with lower TriThiol−APE concentrations (15% TriThiol−15% APE/70% Acr1, Figure 2C), 42% of allyl ether was converted while thiol and acrylate attained 100% conversions. These results are consisted with the previous results[25] produced with a different thiol−ene−acrylate ternary system, in which the thiol and acrylate groups polymerized completely while the ene monomer conversion was highly dependent on the concentration and the propagation and chain-transfer kinetic parameters of thiol and acrylate.

Thermal and Dynamic Mechanical Characterization of TriThiol−APE/Acr1 Networks. Next the acrylate concentration effect on the thermal properties of the polymerized ternary thiol−ene/acrylate polymer network was investigated. The thermal transitions of TriThiol−APE/Acr1 4 mm thick plates were monitored with a DSC. There was no significant change in the glass transition regions recorded by the first and the second heating cycles, the second heating cycles of DSC exotherms were used to obtain glass transition temperatures. Thiol−ene polymers are known to form very homogeneous cross-linked network structures with low glass transition temperatures (T_g) due to the flexibility of the thioether structures in the polymer backbones. On the other hand, multifunctional acrylates form heterogeneous glassy polymers with a wide distribution of dense regions resulting in broad glass transition regions.[2−6] As shown in Figure 3, a TriThiol−APE network plate has a glass transition region between −30 and −15 °C, which shifts to higher temperatures and broadens with Acr1 concentration. The distinct and narrow heat capacity transition of TriThiol−APE becomes broader and less detectable at high acrylate concentration, which introduces heterogeneity into the final network structure. Curve e in Figure 3 clearly shows that the onset of large-scale cooperative segmental motions of a 10% TriThiol−10% APE/80% Acr1 cured network starts at 30 °C and continues until 75 °C. Polymers with more than 70% Acr1 concentration exhibit the features of acrylate homopolymers, nonuniform rigid network structures with kinetically trapped morphologies containing heterogeneously distributed free volumes which extend the glass transition temperature regions up

Table 1. Summary of tan δ_{max}, DSC T_g, and Absorbed Impact Energies of TriThiol−APE/Acr1 Samples as a Function of Acr1 Concentration at Room Temperature

TriThiol−APE/Acr1	tan δ_{max} (°C) (FWHM)	tan δ (FWHM) (°C)	DSC T_g (°C)	energy absorbed (J, at 25 °C)	% impact energy absorption
50% TriThiol−50% APE	−11 (12.9)	12.9	−20	0.41	36
45% TriThiol−45% APE/10% Acr1	−8 (14.2)	14.2	−16	0.46	41
40% TriThiol−40% APE/20% Acr1	−1 (13.5)	13.5	−15	0.56	50
35% TriThiol−35% APE/30% Acr1	7 (17.8)	17.8	−8	0.75	66
30% TriThiol−30% APE/40% Acr1	13 (18.3)	18.3	−2	0.91	81
25% TriThiol−25% APE/50% Acr1	19 (17.3)	17.3	5	0.93	82
20% TriThiol−20% APE/60% Acr1	28 (21.6)	21.6	20	0.71	63
15% TriThiol−15% APE/70% Acr1	37 (24.5)	24.5	31	0.47	42
10% TriThiol−10% APE/80% Acr1	52 (29.2)	29.2	42	0.41	36
5% TriThiol−5% APE/90% Acr1	64 (45.3)	45.3	46	0.39	35
Acr1	79 (88.2)	88.2	59	0.38	34

Table 2. Summary of DSC T_g, tan δ_{max}, the Impact Energy Absorbed, and the % Impact Energy Absorption Results of the Formulations at Room Temperature

formulation	DSC T_g (°C)	tan δ_{max} (°C)	tan δ FWHM (°C)	energy absorbed (J, at 25 °C)	% impact absorption
45% TriThiol−45% APE/10% Acr2	−14	7	8.7	0.53	47
40% TriThiol−40% APE/20% Acr2	−10	12	14.8	0.84	74
37.5% TriThiol−37.5% APE/25% Acr2	−7	13	18.5	0.95	84
35% TriThiol−35% APE/30% Acr2	−4	24	16.5	0.94	83
30% TriThiol−30% APE/40% Acr2	20	39	29.7	failed	
45% TriThiol−45% APE/10% Acr3	−13	8	9.4	0.60	53
40% TriThiol−40% APE/20% Acr3	−9	11	21.8	0.90	80
37.5% TriThiol−37.5% APE/25% Acr3	−6	22	18.9	0.91	81
30% TriThiol−30% APE/40% Acr3	8	44	52.1	failed	
45% TriThiol−45% APE/10% Acr4	−13	4	14.6	0.73	64
40% TriThiol−40% APE/20% Acr4	−11	14	26.6	0.87	77
35% TriThiol−35% APE/30% Acr4	2	32	45.3	failed	
27.5% TriThiol−27.5% APE/45% Acr5	9	21	15.1	0.93	83
25% TriThiol−25% APE/50% Acr5	12	25	18.9	0.82	73
20% TriThiol−20% APE/60% Acr5	20	35	24.3	failed	
27.5% TriThiol−27.5% APE/45% Acr6	6	20	17.2	0.93	82
25% TriThiol−25% APE/50% Acr6	12	26	20.9	0.91	81
20% TriThiol−20% APE/60% Acr6	22	40	25	failed	
35% TriThiol−35% APE/30% Acr7	−2	15	14.0	0.86	76
30% TriThiol−30% APE/40% Acr7	8	23	13.2	1.02	91
25% TriThiol−25% APE/50% Acr7	11	30	14.8	0.81	71

to a range of 100 °C for pure Acr1 (Figure 3, curve f). DSC T_g values are listed in Table 1 for all ternary samples involving Acr1 and TriThiol−APE.

DMA can be used to obtain storage and loss moduli as a function of temperature at a given frequency. The ratio of the storage and loss moduli gives tan δ, a damping term, which relates the ratio of the energy dissipated by heat to the energy stored in the material upon periodic deformation. Previous DMA[11] of thiol−acrylate photopolymerized networks showed that the addition of multifunctional thiols to a multifunctional acrylate increases network homogeneity and reduces the storage modulus and the value of the tan δ peak maximum (tan δ_{max}). DMA results of TriThiol−APE/Acr1 networks as a function of Acr1 concentration are given in Figures 4 and 5. The addition of Acr1 to TriThiol−APE mixtures increases the rubbery modulus of the photocured ternary systems. The rubbery modulus of Acr1 is around 1×10^2 MPa, which is about 5 times higher than that of the TriThiol−APE matrix (Figure 4). A significant increase in the rubbery modulus begins when the concentration of Acr1 reaches a level of at least 40 wt %. Additionally, the transition in storage modulus of pure Acr1 which extends over a range of ∼100 °C reduces to a range of ∼30 °C with the incorporation of 10% TriThiol−10% APE into the network structures. It can be concluded that the contribution from the step-growth reaction process of TriThiol with APE and Acr1 results in a more homogeneous network structure. The chain transfer reaction to thiol from both enes (allyl ether and acrylate) incorporates thioether structures with shortened acrylate sequences providing flexibility and uniform free volume distribution, thereby facilitating the molecular motions in the network. Therefore, as already noted, the ternary systems exhibit a dynamic modulus (E') transition over a much smaller temperature range than pure acrylates. As given in Figure 5, the magnitude of the tan δ peak maximum (tan δ_{max}) increases upon the addition of TriThiol−APE to Acr1. The loss modulus buildup, the decrease in the temperature at tan δ_{max}, and the decrease in fwhm of the tan δ plots in Figure 5 with increasing TriThiol−APE concentration are the direct result of contributions from the step-growth copolymerization process characteristic of thiol−ene reactions. In summary, the DMA results clearly demonstrate the control of the material properties achieved by adjusting the composition of the ternary systems.

Impact Energy Absorption of TriThiol−APE/Acr1 Networks. There has been no previous study dealing with nondestructive impact energy absorption of thiol−ene polymers except for our initial communication on ternary systems.[30] The determination of the energy absorption under nondestructive impact conditions is useful in comparative evaluation of energy dissipation properties of materials used for personal protection.[31] It can be estimated from the difference between a pendulum's rebound height and its original drop height. In the present case, a moderate impact load, 1.13 J, is applied as an impact blow from a weighted pendulum head that is released from a latched position at a fixed height h. An 8 mm thick (two 4 mm plates) rectangular-shaped polymer specimen is positioned at the base. Upon release, the pendulum strikes the sample and rebounds to a height, h'. The results, computed from the difference between h and h', can be used to estimate the impact energy

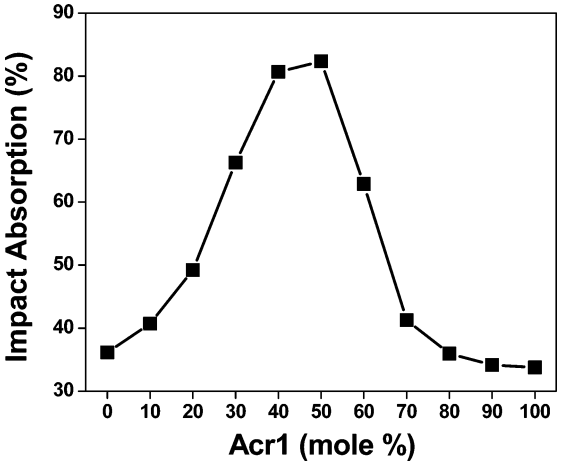

Figure 6. Percent impact absorption plot of 4 mm TriThiol−APE/Acr1 thick plates cured (see Experimental) in air as a function of Acr1 concentration.

absorption of the material. The results of these nondestructive impact tests can be used for making comparisons between different materials under the constraints of the measurement configuration. Percent energy absorption values of the ternary TriThiol−APE/Acr1 plates are plotted in Figure 6 as a function of Acr1 concentration. The photocured ternary samples containing 40 and 50 mol % Acr1 are the most effective at dissipating impact energy at room temperature (Figure 6), absorbing 84% and 86%, respectively, of the impact energy of the striking head. For amorphous polymers, the ability to dissipate energy should increase substantially near the T_g where cooperative molecular motions capable of relieving applied impact stress are activated within the available free volume, resulting in dissipation of the energy by mechanical damping.[34−41] Thus, allowing for differences in frequency between the DMA and nondestructive analysis method, the 40 and 50 mol % acrylate containing samples should be the most energy absorbing near room temperature where both have substantial tan δ values (Figure 5). To confirm a relation between the impact energy absorption efficiency and tan δ plots, energy absorption measurements for three selected ternary samples were conducted as a function of temperature (Figure 7). Again, allowing for frequency differences and resulting temperature shifts due to measurement techniques, the DMA based tan δ plots parallel the energy absorption plots in Figure 7 for the 20%, 50%, and 60% Acr1 sample plates. This certainly indicates a correlation of the molecular relaxation processes inherent to the periodic small deformations of DMA evaluation and the dissipation of a nondestructive impact energy of 1.13 J.

Thermal and Mechanical Characterization of Thiol−Ene/Acrylate Networks. Chemical and monomer structural factors such as the bridging groups between functional groups and the number of reactive groups per molecule have a distinct influence on the network heterogeneity.[42−45] For example, it has been shown that (meth)acrylates with a high functionality and/or low molecular weight bridging groups between reactive double bonds lead to more heterogeneous networks with regions where stresses can potentially result in material fracture and failure.[42−45] To analyze structural factors affecting the energy absorption of these highly cross-linked ternary systems, acrylates with variation in structure and functionality (Chart 2) were evaluated in place of Acr1. Table 2 and Figure 8 summarize the impact absorption results of ternary systems incorporating the acrylates in Chart 2 as a function of DSC T_g and DMA tan δ_{max} values. First, as shown in Figure 8A,B, it is clear that ternary samples

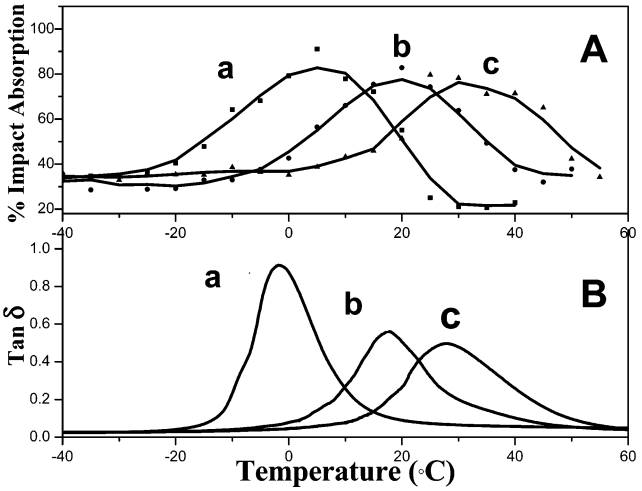

Figure 7. Percent impact absorption (A) and DMA tan δ (B) plots of TriThiol−APE/Acr1 ternary thick plates cured (see Experimental) in air as a function of temperature: (a, ■) 40% TriThiol−40% APE/20% Acr1, (b, ●) 25% TriThiol−25% APE/50% Acr1, and (c, ▲) 20% TriThiol−20% APE/60% Acr1. Solid lines in the percent impact absorption plot (A) are achieved by Gaussian curve fitting.

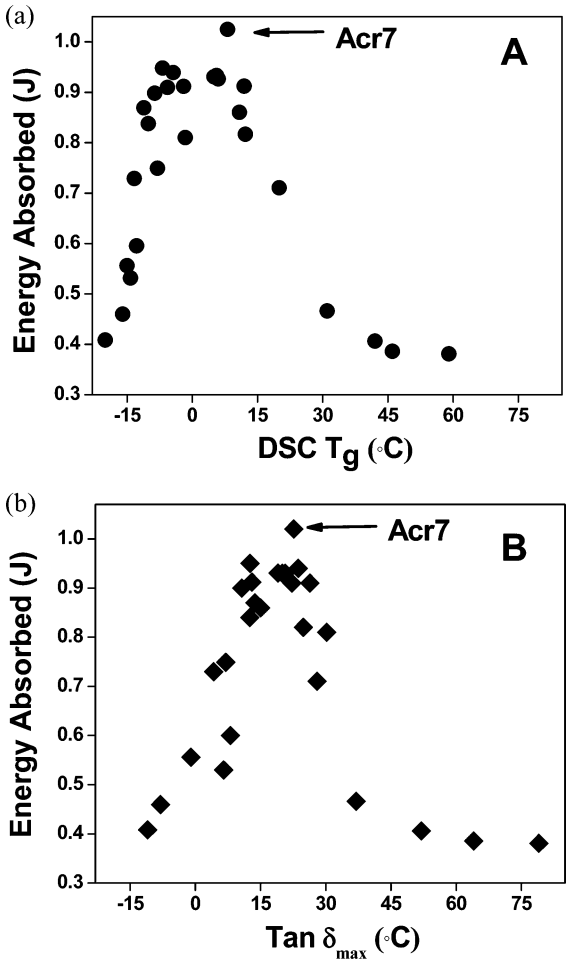

Figure 8. Absorbed energy vs (A) DSC T_g and (B) temperature at DMA tan δ_{max} plots of ternary systems given in Tables 1 and 2. Thick plates cured (see Experimental) in air.

with different acrylate monomers incorporated at various concentrations exhibit energy absorption that depends on matrix mechanical transition maxima; samples with DSC T_g between −5 and 20 °C or tan δ_{max} values around 10−25 °C absorb more than 80% of the impact energy. Of course, the functionality

and monomer structure dictate what concentration of acrylate is required to achieve a transition at a given temperature. For example, consider the results in Table 2 for Acr2 and Acr5 (both triacrylates); a network formed from a certain concentration of Acr2 (e.g., 40%) has a transition maxima at higher temperature than a network formed from a slightly higher concentration of Acr5 (e.g., 45%). This results from the ethoxy linkage of Acr5 which is flexible and provides a higher molecular weight bridge between acrylate groups. A similar difference is seen for Acr3 vs Acr6, both of which are tetraacrylates. The effect of functionality is most readily seen by comparing the relatively low concentrations needed to achieve a given transition temperature for the pentafunctional Acr6 compared to the other acrylates with lower functionality. It is the combination of chemical structure and the number of reactive acrylates that dictates the concentration required to achieve a given transition temperature. We point out one other important consideration in network formation involving thiol−enes and some of the acrylates. In each case for Acr 2−Acr 6 (Table 2), as the concentration reaches a critical value, the plate experiences fracture, and hence failure, upon impact. The networks for which fracture failure occur are characterized in each case by a critical acrylate concentration such that the tan δ plots have broader fwhm values and a temperature at tan δ_{max} greater than ~30 °C. The broader tan δ plots are indicative of heterogeneous glassy networks (at room temperature) that have high-density weak spots, which upon impact can lead to matrix failure.[33] Interestingly, acrylates Acr2−Acr6 all have functionality of three or greater, relatively low molecular weight bridging groups, and no structural groups that can absorb energy via molecular group sub-T_g motions.

Up until now, we have not discussed the results obtained for Acr1 and Acr7 with respect to network structure and impact energy absorption and fracture failure. We first point out that networks formed using Acr1 or Acr7 did not exhibit fracture failure upon the 1.13 J impact, even for samples with up to 50 mol % of acrylate groups. Moreover, the 40% Acr7 sample has significantly higher energy absorption (Figure 8A,B) than the other ternary samples with similar T_g. Both Acr1 and Acr7 have molecular groups, the methyl groups on Acr1 and the bisphenol A structural group for Acr7, which are expected to have sub-T_g relaxations which can limit fracturing.

Hartmann et al.[38] showed that a single impact pulse consists of a wide distribution of frequencies. They used a Fourier analysis to obtain a complete frequency spectrum of the impact energy and successfully recorded frequencies as high as 200 Hz for a typical impact. Considering the potential for high-frequency molecular relaxations that can ameliorate fracture, it is not surprising that the samples prepared from Acr1 or Acr7 did not fracture. Additionally, Acr7 is difunctional, which upon polymerization in the absence of other components yields polymer networks with lower network heterogeneity than networks formed with trifunctional acrylates and thus a reduced propensity to fracture.[42] We were not able to detect sub-T_g β-relaxation peak(s) via DMA for samples prepared from Acr1; however, such relaxations are broad and often difficult to identify. We were able to detect sub-T_g mechanical transitions for the samples based on Acr7 (Figure 9). The observed peaks around −20 and −80 °C in the DMA plot in Figure 9 of the sample containing Acr7 indicate the motion of secondary groups. Bulky bis-phenol groups apparently provide enough free volume within the network structure for restricted rotation of phenyl groups in the chain. This motion of bis-phenol A groups is well-known to have characteristic relaxations around −80 °C,[34−41]

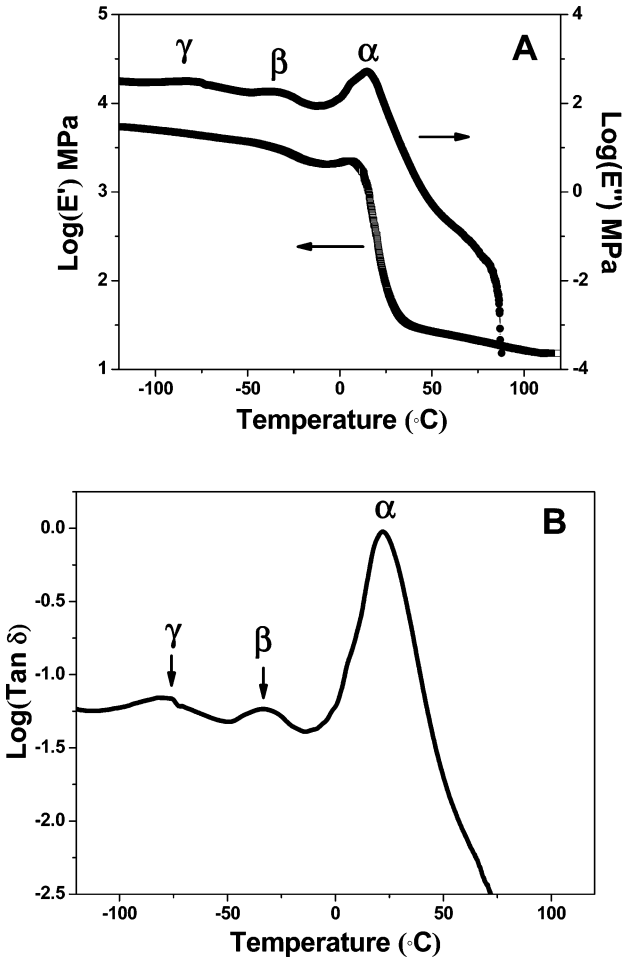

Figure 9. DMA results of 30% TriThiol−30% APE/40% Acr7 ternary sample cured (see Experimental) in air. (A) Storage and loss moduli and (B) tan δ plots obtained at a scan rate 2 °C/min.

commensurate with the peak in Figure 9B. We speculate that the indicated β- and γ-relaxation peaks in Figure 9A,B are the primary reason for the considerably high impact energy absorption of the sample containing Acr7 at room temperature. This speculation is consistent with considerable theoretical[34] and experimental[35−41] reports correlating the secondary relaxation peaks in DMA plots with the impact strength of glassy materials such as epoxides, polystyrene, and polycarbonate. Specifically, Ochi et al.[36] showed that the impact properties of BPA-based epoxide polymers are directly correlated to a β-relaxation process as well as the onset of the motion at T_g and the cross-link density of the matrix. It has been shown that low-temperature secondary relaxations can shift to room temperature due to high-frequency impact forces and become effective in absorbing and dissipating impinging energy.[38−41]

Thiol−Ene/Acrylate and Thiol/Acrylate Comparison. As mentioned in the Introduction, thiol monomers have also been added to acrylates,[8,11,27−29] resulting in narrowing of the tan δ vs temperature plots and lowering of the glass transition temperature. Addition of thiol to acrylates provides the opportunity to adjust the T_g depending on the amount of multifunctional thiol monomer added. In an attempt to define any expanded role of the ene monomer APE in ternary systems, selected formulations were prepared with/without the presence of APE. The concentrations of TriThiol in Acr1 and Acr7 have been adjusted to obtain a tan δ_{max} around 15−25 °C. As shown in Figure 10, the samples fabricated from 30% TriThiol/70% Acr1 and 40% TriThiol/60% Acr7 give T_gs comparable to two

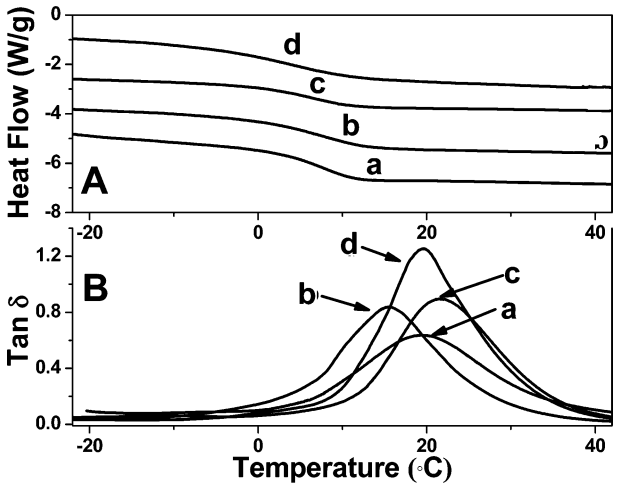

Figure 10. DSC heat flow curves (A) and DMA tan δ plots (B) of (a) 25% TriThiol−25% APE/50% Acr1, (b) 30% TriThiol/70% Acr1, (c) 30% TriThiol−30% APE/40% Acr7, and (d) 40% TriThiol/60% Acr7.

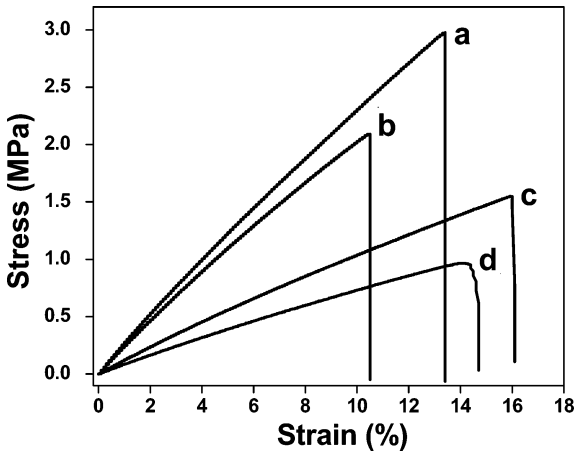

Figure 11. Tensile stress vs percent elongation plots of (a) 25% TriThiol−25% APE/50% Acr1, (b) 30% TriThiol/70% Acr1, (c) 30% TriThiol−30% APE/40% Acr7, and (d) 40% TriThiol/60% Acr7, obtained with tensile testing machine, at crosshead speed of 25 mm/min. Films cured (see Experimental) in air.

ternary systems, 25% TriThiol−25% APE/50% Acr1 and 30% TriThiol−30% APE/40% Acr7, respectively. The impact analyses of these four samples are in the same range, with more than 80% of the impact energy absorbed in each case. In order to elucidate any differences in material properties between these thiol−acrylate and thiol−ene/acrylate samples, tensile properties of these four samples (1 mm thick) were measured. Stress vs strain plots in Figure 11 shows that all samples break in a brittle manner without yielding, and elongations are low (10−15%) due to the thermoset nature of the matrices. The stress at break values for trifunctional Acr1 containing samples are higher than their difunctional Acr7 counterparts, which is due to the higher macroscopic cross-link density afforded by Acr1 (Figure 11, curves a and b). The Acr7-based networks have higher elongation at break, perhaps attributable in part to the Acr7's higher molecular weight per double compared to Acr1. In the ternary systems fine-tuning physical properties can be achieved by altering the ratios of the three components. Differences that may occur between binary and ternary systems are under continued investigation.

Conclusions

This study provides critical insight into the physical and thermomechanical properties of thiol−ene/acrylate-based ternary systems. Owing to differences in the polymerization mechanism of acrylate and thiol−ene, ternary thiol−ene/acrylate systems exhibit a variety of properties depending on composition and the acrylate chemical structure. Kinetic analysis of these ternary systems shows that acrylate monomer reaches 100% conversion in all the mixtures upon addition of thiol−ene due to acrylate homopolymerization and copolymerization with thiol monomer. However, thiol and ene monomer conversions are dependent on their concentrations in the system. Acrylate incorporation in the thiol−ene matrix increases the rubbery modulus of the system while decreasing the magnitude of the tan δ peak due to the heterogeneous distribution of cross-linked regions. The glass transition of the final matrices can be adjusted by altering the composition of the system. The energy absorption upon impact of these ternary thermoset polymers correlates with the tan δ_{max} and chemical structure of the components. To obtain substantial energy absorption without material fracture, the network should be uniform, as identified by the narrowness of the tan δ vs temperature plots, to avoid fracture that begins at high-density sites in the matrix. Relaxations lying below tan δ_{max}, such as those seen for the system containing a bisphenol-based acrylate, result in exceptional enhancement of energy absorption properties. Finally, the presence of the ene monomer along with acrylates in the ternary provides a potential additional route for fine-tuning network physical properties.

Acknowledgment. This work was supported by the MRSEC Program of the National Science Foundation under Award DMR 0213883 and Fusion UV Systems, Inc. We also thank Perstorp, Bruno Bock, Ciba Specialty Chemicals, Sartomer Company and Cytec Surface Specialties for providing samples.

References and Notes

(1) Roffey, C. G. *Photogeneration of Reactive Species for UV Curing*; John Wiley and Sons: New York, 1997.
(2) Kloosterboer, J. G. *Adv. Polym. Sci.* **1988**, *84*, 1−61.
(3) Kloosterboer, J. G.; Van de Hei, G. M.; Boots, H. M. J. *Polym. Commun.* **1984**, *25*, 354−357.
(4) Bowman, C. N.; Anseth, K. S. *Macromol. Symp.* **1995**, *93*, 269−276.
(5) Dusek, K. In *Developments in Polymerization*; Harvard, R. N., Ed.; Applied Science: London, 1982; Vol. 3, Chapter 4.
(6) Dusek, K.; Galina, H.; Mikes, J. *Polym. Bull.* **1980**, *3*, 19−25.
(7) Chiou, B.; Khan, S. A. *Macromolecules* **1997**, *30*, 7322−7328.
(8) Morgan, C. R.; Magnotta, F.; Ketley, A. D. *J. Polym. Sci., Part A* **1977**, *15*, 627−645.
(9) Jacobine, A. F. In *Radiation Curing in Polymer Science and Technology III*: *Polymerization Mechanisms*; Fouassier, J. D., Rabek, J. F., Eds.; Elsevier: London, 1993; Chapter 7, pp 219−68.
(10) Hoyle, C. E.; Lee, T. Y.; Roper, T. *J. Polym. Sci.* **2004**, *42*, 5301−5338.
(11) Cramer, N. B.; Bowman, C. N. *J. Polym. Sci., Part A* **2001**, *39*, 3311−3319.
(12) Cramer, N. B.; Reddy, S. K.; Lu, H.; Cross, T.; Raj, R.; Bowman, C. N. *J. Polym. Sci., Part A* **2004**, *42*, 1752−1757.
(13) Reddy, S. K.; Cramer, N. B.; Cross, T.; Raj, R.; Bowman, C. N. *Chem. Mater.* **2003**, *15*, 4257−4261.
(14) Cramer, N. B.; Bowman, C. N. *Polym. Prepr.* **2003**, *44*, 17−18.
(15) Lu, H.; Stansbury, J. W.; Bowman, C. N. *Dent. Mater.* **2005**, *21*, 1129−1136.
(16) Cramer, N. B.; Scott, C. P.; Bowman, C. N. *Macromolecules* **2002**, *35*, 5361−5365.
(17) Hoyle, C. E.; Hensel, R. D.; Grubb, M. B. *J. Polym. Sci., Part A* **1984**, *22*, 1865−1873.
(18) Reddy, S. K.; Cramer, N. B.; O'Brien, A. K.; Cross, T.; Raj, R.; Bowman, C. N. *Macromol. Symp.* **2004**, *206*, 361−374.
(19) Cramer, N. B.; Reddy, S. K.; Cole, M.; Hoyle, C. E.; Bowman, C. N. *J. Polym. Sci., Part A* **2004**, *42*, 5817−5826.
(20) Cramer, N. B.; O'Brien, A. K.; Bowman, C. N. *J. Polym. Sci., Part A* **2006**, *44*, 2007−2014.
(21) Cramer, N. B.; Reddy, S. K.; O'Brien, A. K.; Bowman, C. N. *Macromolecules* **2003**, *36*, 7964−7969.
(22) Cramer, N. B.; Davies, T.; O'Brien, A. K.; Bowman, C. N. *Macromolecules* **2003**, *36*, 4631−4636.

(23) Lee, T. Y.; Roper, T. M.; Jonsson, E. S.; Guymon, C. A.; Hoyle, C. E. *Macromolecules* **2004**, *37*, 3606−3613.
(24) Reddy, S. K.; Cramer, N. B.; O'Brien, A. K.; Bowman, C. N. *Macromolecules* **2006**, *39*, 3673−3680.
(25) Reddy, S. K.; Cramer, N. B.; O'Brien, A. K.; Bowman, C. N. *Macromolecules* **2006**, *39*, 3681−3687.
(26) Okay, O.; Reddy, S. K.; Bowman, C. N. *Macromolecules* **2006**, *38*, 4501−4511.
(27) Gush, D. P.; Ketley, A. D. *Mod. Paint Coat.* **1978**, *68*, 58−66.
(28) Eisele, G.; Fouassier, J. P.; Reeb, R. *J. Polym. Sci., Part A* **1997**, *35*, 2333−2345.
(29) Lecamp, L.; Houllier, F.; Youssef, B.; Bunel, C. *Polymer* **2001**, *42*, 2727−2736.
(30) Senyurt, A. F.; Wei, H.; Philips, B.; Cole, M.; Nazarenko, S.; Hoyle, C. E.; Piland, S.; Gould, T. *Macromolecules* **2006**, *39*, 6315−6317.
(31) Craig, R. G.; Godwin, W. C. *J. Oral. Rehab*. **2002**, *29*, 146−150.
(32) Pritchard, G.; Rhoades, G. V. *Mater. Sci. Eng*. **1976**, *26*, 1−11.
(33) Van der Sanden, M. C. M.; Meijer, H. E. H. *Polymer* **1993**, *34*, 5063−5072.
(34) Wada, Y.; Kasahara, T. *J Appl. Polym. Sci.* **1967**, *11*, 1661−1665.
(35) Vincent, P. I. *Polymer* **1974**, *15*, 111−116.
(36) Ochi, M.; Iesako, H.; Nakajima, S. *J. Appl. Polym. Sci. (Phys.)* **1986**, *24*, 251−261.
(37) Shimbo, M.; Nishitani, N.; Takahama, T. *J. Appl. Polym. Sci.* **1984**, *29*, 1709−1721.
(38) Hartmann, B.; Lee, G. F. *J. Appl. Polym. Sci*. **1979**, *23*, 3639−3650.
(39) Boyer, R. F. *Polymer* **1976**, *17*, 996−1008.
(40) Sacher, E. *J. Macromol. Sci., Phys*. **1975**, *B11*, 403−410.
(41) Boyer, R. F. *Polym. Eng. Sci.* **1968**, *8*, 161−185.
(42) Elliott, J.; Bowman, C. N. *Macromolecules* **2001**, *34*, 4642−4649.
(43) Anseth, K. S.; Bowman, C. N. *Chem. Eng. Sci*. **1994**, *41*, 2207−2217.
(44) Elliott, J.; Bowman, C. N. *Polym. React. Eng.* **2002**, *10*, 1−19.
(45) Elliott, J.; Bowman, C. N. *Macromolecules* **1999**, *32*, 8621−8628.

MA062534B